Determination of molecular torsion angles using nuclear singlet relaxation

Supporting information

Michael C. D. Tayler, Sabrina Marie, A. Ganesan, Malcolm H. Levitt*
School of Chemistry, University of Southampton, SO17 1BJ, Southampton, UK

Contents

S.1 Samples

The following preparations give details on the synthetic route to the d_1-Phe isotopolog starting from racemic phenylalanine. Deuteration at the C^α position was performed first, followed by substitutions at the amino and carboxylic acid groups. The other isotopologs were produced in an analogous manner, each time starting from either d_0 or d_5 DL-phenylalanine (obtained commercially).

DL-[α^2H] phenylalanine

According to the procedure by Mitulovi *et al.* [1]: salicylaldehyde (35 μl, 0.33 mmol) was added to a solution of DL-phenylalanine (280 mg, 1.70 mmol) in acetic acid (OD, 10 ml). The solution was heated for one hour at 100 °C before concentration under reduced pressure. D_2O (98%, 2 ml) was added and the solution stirred for 15 minutes. The solution was then diluted (D_2O), treated with charcoal, filtered, and evaporated under reduced pressure to yield DL-[α^2H] phenylalanine (198 mg, 70%, *d*-97%) as a fine white powder.

^{1}HNMR, 300 MHz in D_2O: δ/ppm 3.06 and 3.23 (1H, d, J = 14 Hz, CH_2 (β)/(β')), 7.25-7.40 (5H, m, Ph)

***N,N*-Phthaloyl [α^2H] phenylalanine**

Adapted from the procedure of Achmatowicz *et al.* [2]: Triethylamine (42 μl, 0.3 mmol) and phthalic anhydride (52 mg, 0.33 mmol) were added to a solution of [α^2H] phenylalanine (52 mg, 0.3 mmol) in toluene (5 ml). The reaction mixture was refluxed overnight, then evaporated under vacuum and the residue washed (1M HCl) and triturated with water several times to give a white solid: *N,N*-phthaloyl [α^2H] phenylalanine (75 mg, 78 %).

^{1}HNMR, 300 MHz in $CDCl_3$:; δ/ppm 3.60 (2H, s, CH_2), 7.14-7.20 (5H, m, Ph), 7.67-7.80 (4H, m, Phth)

***N,N*-Phthaloyl [α^2H] phenylalanine methyl ester ('d_1-Phe' isotopolog)**

This was prepared according to the procedure of Yu *et al.* [3]: Under argon at −13 °C, thionyl chloride (175 μl, 2.4 mmol) was added dropwise to a solution of *N,N*-phthaloyl [α^2H] phenylalanine (120 mg, 0.4 mmol) in methanol (5 ml, anhydr). The solution was stirred overnight at room temperature. After concentration the mixture was purified by flash chromatography (eluent Hexane/EtOAc 85:15) to yield the product (90 mg, 72%, white solid).

^{1}HNMR, 300 MHz in $CDCl_3$; δ/ppm 3.54 and 3.62 (1H, d, J = 14 Hz, CH_2 (β)/(β')), 3.79 (3H, s, MeO), 7.17-7.19 (5H, m, Ph), 7.67-7.80 (4H, m, Phth)

Each sample was dissolved to c. 60 mM in d_4-methanol (*d*-99.96%). After transferring the solutions into 5 mm outer-diameter NMR tubes equipped with Young valves, the samples were thoroughly degassed (freeze-pump-thaw, typically 5-6 cycles) to remove the majority of dissolved oxygen, and then sealed.

S.2 NMR methods

The experiments were performed at a working field of 9.4 T using a Varian InfinityPlus NMR spectrometer equipped with a 5 mm HX liquid probe. A constant air purge was maintained across the probehead throughout; (i) to ensure the constant temperature of the sample, (ii) as a means to reduce stress on the probe coils during the period of continuous-wave singlet spin locking.

To acquire the relaxation data we used the following procedure: (i) we recorded the one-pulse ^{1}H spectrum, and located the resonances belonging to the C$^\beta$ proton pair; (ii) T_1 for these protons was then determined from longitudinal relaxation measurements made by inversion-recovery, where inversion of the magnetization was carried out over the whole spectrum; (iii) we employed the scheme proposed by Sarkar *et al.*, ([4], as reproduced in Figure 1), to excite, store, and subsequently detect the H$^\beta$H$^{\beta'}$ singlet population and following that infer the relaxation constant T_S.

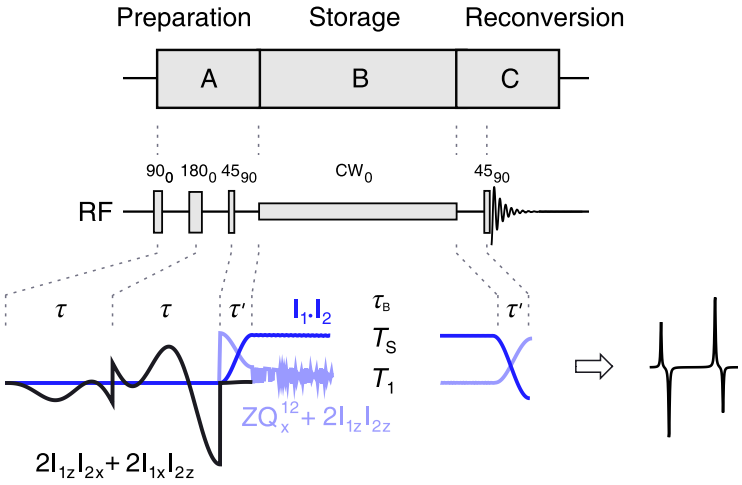

Figure 1: Sarkar *et al.* pulse sequence for measurement of the singlet relaxation time constant, T_S. The uppermost part of the figure displays a schematic view of the sequence, containing three distinct elements which we have labelled A, B and C – pulses on the ^{1}H channel are show immediately below: (A), equilibrium thermal magnetization is transferred *via* antiphase coherences into a mixture of zero-quantum ($ZQ_x \propto I_{1+}I_{2-} + I_{1-}I_{2+}$) and longitudinal two-spin-order ($2I_{1z}I_{2z}$) terms. To maximize this conversion the spin-echo duration is set according to the H$^\beta$H$^{\beta'}$ scalar coupling ($2\tau = 1/|2J_{\beta\beta'}|$ being a very good estimate). The zero-quantum term is then permitted to evolve into an isotropic component $\mathbf{I}_1 \cdot \mathbf{I}_2 \propto 3\,|S_0^{12}\rangle\langle S_0^{12}| - (|T_{-1}^{12}\rangle\langle T_{-1}^{12}| + |T_0^{12}\rangle\langle T_0^{12}| + |T_{+1}^{12}\rangle\langle T_{+1}^{12}|)$ that represents the long-lived state, where the second evolution period is given approximately by $\tau' \approx \pi/|2(\omega_1^0 - \omega_2^0)|$; (B), continuous-wave (CW) spin locking is applied. This has the effect of isolating the resulting state of singlet population from coherent evolution processes, so the population may change only as a consequence of relaxation, the process with which T_S is identified. In our case a CW locking strength of 2.0 kHz ($\gg |\omega_1^0 - \omega_2^0|/2\pi$) was used, centred approximately at the average chemical shift of the two H$^\beta$ resonances; (C), remanent singlet population at the end of the lock is converted back into observable antiphase magnetization through the reverse application of element (A). This results in the characteristic [antiphase] shape of the doublets. We repeat the sequence for various τ_B to generate an array of spectra whose intensity $A(\tau_B)$ is fitted to the relaxation factor, $\ln(A/A(0)) = -\tau_B/T_S$, obtaining the decay constant T_S. The bottom plot follows the simulated trajectories of the sum antiphase magnetization, 'x' zero-quantum and long-lived-singlet population operators throughout time.

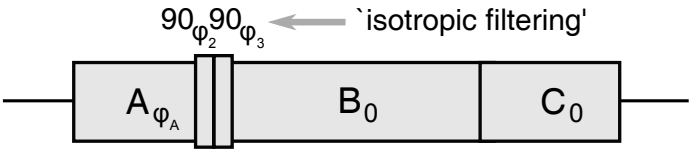

Figure 2: Diagrammatic representation of the isotropic filter. The 12-step phase cycle shown in Table 1 is used to result in only signal pathways passing through the singlet state appearing in the final spectra.

The NMR signals from the pure singlet-derived terms were obtained using an *isotropic filtration* phase cycle. This refers to the prodecure described by Pileio *et al.* [5] where spectra from a series of phase-shifted NMR experiments are added uniformly together to average out all components of the NMR signal that [at some specified time point during the sequence] do not pass through rotational invariants. In this case the invariant is the long-lived singlet population. Terms that are suppressed thus include signals from the solvent, and non-equilibrated triplet populations, both of which else contaminate the spectra at short ($\tau_B < T_1(\mathrm{H}^\beta)$) spin locking times. We implemented the phase cycle using a slightly modified pulse sequence to that shown in the previous figure, which involved inserting two 90° pulses between blocks A and B (Figure 2). We let this modified sequence be denoted $(A)_{\varphi_A} - (90)_{\varphi_2} - (90)_{\varphi_3} - (B)_{\varphi_B} - (C)_{\varphi_C}$, so that φ_A *etc.* marks the incremental phase additions to each of the pulses within each corresponding block. The so-called 'tetrahedral' 12-step phase cycle given in Table 1 then results in excellent supression of non-singlet-derived peaks in the final spectrum. The fact is affirmed by the low standard errors (r.m.s.d. = less than 2 %) measured in our fittings of the singlet decay curves.

expt.	φ_A	φ_2	φ_3
1	0	0	180
2	120	0	180
3	240	0	180
4	109.47	109.47	180
5	229.47	109.47	180
6	349.47	109.47	180
7	109.47	229.47	300
8	229.47	229.47	300
9	349.47	229.47	300
10	109.47	229.47	60
11	229.47	229.47	60
12	349.47	229.47	60

Table 1: 12-step 'tetrahedral' isotropic filtration phase cycle. All angles are in degrees.

S.3 Outline derivation of Equation [2]

It is well-known for a pair of magnetically-equivalent spin-1/2 nuclei that if the NMR relaxation is dominated by the direct-dipole coupling mechanism then the singlet population – represented by the irreducible spherical tensor operator T_{00}^{12} – is an eigenvector of the two spin Liouvillian propagator. ($\mathrm{T}_{00}^{12} \propto N[|S_0^{12}\rangle\langle S_0^{12}| - \frac{1}{3}(|T_{-1}^{12}\rangle\langle T_{-1}^{12}| + |T_0^{12}\rangle\langle T_0^{12}| + |T_{+1}^{12}\rangle\langle T_{+1}^{12}|)] \propto \mathbf{I}_1 \cdot \mathbf{I}_2$)

In that case both the singlet state and longitudinal spin-lattice relaxation rates are simply given by the diagonal elements of the total dipole-dipole relaxation superoperator: *i.e.*

$$(T_S)_{\mathrm{DD}}^{-1} \;=\; -(\mathrm{T}_{00}^{12}|\hat{\Gamma}_{\mathrm{DD}}|\mathrm{T}_{00}^{12}) \;=\; 0 \tag{1}$$

$$(T_1)_{\mathrm{DD}}^{-1} \;=\; -(\mathrm{I}_{1z}+\mathrm{I}_{2z}|\hat{\Gamma}_{\mathrm{DD}}|\mathrm{I}_{1z}+\mathrm{I}_{2z}) \;=\; \frac{3}{10}b_{12}^2\big(j(\omega^0)+4j(2\omega^0)\big). \tag{2}$$

$$\Big(\text{with} \qquad \hat{\Gamma}_{\mathrm{DD}} \;=\; -\frac{6}{5}b_{12}^2\sum_{\mu=-2}^{2}(-)^{\mu}\,j(\mu\omega^0)\,\hat{\mathrm{T}}_{2\mu}^{12}\hat{\mathrm{T}}_{2-\mu}^{12}\Big) \tag{3}$$

in which $j(\omega)$ signifies the unnormalized second-rank spectral density function, $b_{12} = \hbar^2\gamma_j\gamma_k\mu_0/4\pi r_{12}^3$ is the strength of the internuclear dipole coupling, and each $\hat{\mathrm{T}}_{2\mu}^{12}$ denotes one of the irreducible rank-2 spherical tensor operators (as commutators) formed by coupling spins 1 and 2. $T_S \gg T_1$ implies that the singlet state is 'long-lived'.

Consider the presence of a third spin. (*c.f.*, one of the *ortho* ring protons in d_1-Phe) It is known that the singlet population $\mathbf{I}_1\cdot\mathbf{I}_2$ can still be approximate to a Liouvillian eigenvector despite the inherent sources of spin relaxation *provided* that (i) the dipole couplings to the third nucleus ('j', say) satisfy $b_{1j},\, b_{2j} \ll b_{12}$ and (ii), provided the scalar couplings to it are suitably small [6]. The resulting relaxation rates will then be predicted by the first-order matrix elements of the total relaxation superoperator:

$$(T_S)_{\mathrm{DD}}^{-1} \;\approx\; -(\mathrm{T}_{00}^{12}\,|\,\hat{\Gamma}_{\mathrm{DD}}^{\mathrm{total}}\,\mathrm{T}_{00}^{12}) \;=\; \frac{1}{5}\Big(b_{13}^2+b_{23}^2-2b_{13}b_{23}P_2(\cos\beta_{12,23})\Big) \times\big(j(0)+2j(\omega^0)+2j(2\omega^0)\big) \tag{4}$$

where $P_2(\cos\beta_{12,23})$ is the rank-2 Legendre polynomial involving the relative principal orientation of the two coupled tensors. In general the superoperator takes the form

$$\hat{\Gamma}_{\mathrm{DD}}^{\mathrm{total}} \;=\; -\frac{6}{5}\sum_{jk,lm} b_{jk}b_{lm}\,P_2(\cos\beta_{jk,lm})\sum_{\mu=-2}^{2}(-)^{\mu}\,j(\mu\omega^0)\,\hat{\mathrm{T}}_{2\mu}^{jk}\hat{\mathrm{T}}_{2-\mu}^{lm} \tag{5}$$

Subsequent external spins that are not strongly coupled to each other will give independent contributions to the relaxation rates, so can be summed over all spin pairs. Assuming T_1 remains dominated by Equation 2 above, this first-order estimate for the relaxation leads to Equation [2] given in the main article.

N.B. this form is in accordance with the discussions made by Grant and Vinogradov on long-lifetime states in multi-spin systems.[7] Like they note, Eqn 4 predicts that the singlet relaxation rate remains small when: (i) the out-of-pair dipolar couplings are parallel ($\beta_{12,23} \approx 0$) and similar in magnitude ($b_{13} \approx b_{23}$); (ii) when the external spin is at large radius, decreasing in the inverse-eighth power at leading distance order. As a result nuclei at long range can be safely neglected from the relaxation treatment.

It is interesting to note this theory predicts the singlet relaxation rate becomes large compared to T_1 at longer correlation times, due to the $j(0)$ component. We will outline the more detailed and theoretical discussion of such results in a forthcoming publication.

S.4 Notes on calculations and Figs. 2 and 3 of the main article

S.4.1 Mechanisms of relaxation

The experimentally-measured time constant $T_S = 51 \pm 2$ s for the d_6-Phe isotopolog supports how mechanisms other than pure direct-dipole relaxation – for instance, the direct-dipole/CSA cross-correlations – have only a weak influence on the singlet state lifetime. As a result our theoretical treatments of T_S are restricted to the analysis of direct-dipole relaxation, neglecting the cross-correlated H^{β}-CSA–$H^{\beta}H^{\beta'}$-dipolar and CSA-CSA terms.

This simplification can be justified comparing the magnitude of Equation 4 with the analogous CSA-DD contribution. Briefly, the latter scales as

$$(T_S)^{-1}_{\mathrm{DD-CSA}} \quad \propto \quad b_{12}\Big|\Delta\sigma_1 P_2(\cos\beta_{12,1}) - \Delta\sigma_2 P_2(\cos\beta_{12,2})\Big| j(\omega^0) \qquad (6)$$

which approximates to zero by argument of the local symmetry of the methylene group [8, 9]. (here $\Delta\sigma_1$, $\Delta\sigma_2$ refer to the principal values of axial CSA tensors on the methylene protons 1 and 2, respectively, each axis making angles $\beta_{12,1}$, $\beta_{12,2}$ with the internuclear vector $\boldsymbol{r}_1 - \boldsymbol{r}_2$). The contribution to T_1 scales as the sum, rather than the difference of the CSA tensors as above, but remains small in comparison to the autocorrelated $H^{\beta\beta'}$ dipolar relaxation term. The yet-weaker CSA-CSA correlations can be neglected in estimations of both T_S and T_1 in accordance with discussions given in ref. [10].

Direct-dipole and scalar relaxation mechanisms caused by the presence of deuterium nuclei were expected not to be significant, and were completely neglected from simulations in our simplified treatment.

S.4.2 Numerical simulations

d_1-Phe: Figure 2 in the main text shows curves predicting T_S/T_1 for the C^{β} protons as a function of the ring torsion in two different motional regimes: (i) the solid curve indicates the relaxation rate ratio assuming a geometry static

on the correlation timescale of molecular rotation, τ_c^{DD}, whilst (ii) the dashed curve simulates 180° rotational flips of the ring that occur much faster than τ_c^{DD}.

In the static case, both T_S and T_1 were estimated using the perturbation approach *c.f.* Eqn 4 as a sum of direct-dipole contributions only from the two *ortho* phenyl protons; the other protons of the ring being too far away to make significant dipolar rate contributions in the first-order approximation. For the fast-flipping model an identical method was adopted, however, in this case using a Liouvillian propagator $\hat{\Gamma}_{\mathrm{DD}}^{\mathrm{total}}$ constructed from the conformationally-averaged dipolar Hamiltonians to represent the time-effective relaxation for ring flipping occuring at rates $\gg 1/\tau_c^{\mathrm{DD}}$,

$$\textit{viz.} \qquad [\mathscr{H}_{\mathrm{DD}}]^{\mathrm{flipping}} = \Big(\mathscr{H}_{\mathrm{DD}}(\varphi_{\beta\gamma}) + \mathscr{H}_{\mathrm{DD}}(\varphi_{\beta\gamma} + 180^\circ)\Big)/2 \qquad (7)$$

It is important to stress the validity of the 1st-order perturbation approach. Comparison of the rates with those obtained using *Liouvillian eigenvalue analysis*, ([6] an exact method, involving diagonalization of the Liouvillian propagator to infer the eigenoperators and associated relaxation rates), show less than a 1% deviation in both $1/T_1$ and $1/T_S$ for all values of the angle $\varphi_{\beta\gamma}$.

For d_5**-Phe** the effects of dipolar relaxation involving the C^α proton were modeled. Since in this case there exist scalar couplings between the methylene protons and the 'external' spin it is in general not true that $\mathrm{T}_{00}^{\beta\beta'}$ should be approximate to a Liouvillian eigenvector [7]. The relaxation rates were thus modeled using Liouvillian eigenvalue analysis, (Figure 3, main article), for the proton three-spin system. The significance of the ${}^3J_{\alpha\beta}$ 'out-of-pair' scalar couplings in the relaxation is expressed in the figure on page S9.

S.4.3 Geometry

In deriving each of the relaxation rates we used values for the dipolar coupling strengths typical of the bond lengths and bond angles found in phenylalanine as determined by neutron experiments.[13] These figures agree with standard bond lengths and angles. The range of relaxation rates obtained when the bond distances are rounded to the nearest three significant figures allow a precision of ± 5% to be placed on the curves in Figure 2; recall, at long range there is a sensitive $1/\mathrm{distance}^8$ dependence in the positions of nuclei external from the singlet pair.

S.4.4 Field dependence of relaxation

The molecular rotational correlation time was estimated from the T_1 measured for d_6-Phe assuming a dominant dipole-dipole spin-lattice relaxation mechanism. The resulting value $\tau_c^{\mathrm{DD}} = 24$ picoseconds indicates the molecule is well-within the extreme-narrowing regime so the ratio T_S/T_1 should be completely

independent of the rotational correlation time in accordance with §S.3.

However, it is important not to forget the importance of chemical-shift-induced relaxation effects, most notably the CSA-CSA correlations, that may be B^0 dependent and therefore manifest at higher field strengths.

S.4.5 Computational details

The numerical simulations were performed using a scratch-built program written in *Mathematica* running under extensive use of the 'mPackages' spin operator and superoperator routines. [14, 15]

References

[1] Mitulovi, G.; Lämmerhofer, M.; Maier, N. M.; Lindner, W. J. *Labelled Compd. Radiopharm.* **2000**, 43, 449-461.

[2] Achmatowicz, M.; Szumna, A.; Zielinski, T.; Jurczak, J. *Tetrahedron* **2005**, 61, 9031-9041.

[3] Fu, Y.; Xu, B.; Zou, X.; Ma, C.; Yang, X.; Mou, K.; Fu, G.; Lü, Y.; Xu, P. *Bioorg. Med. Chem. Lett.* **2007**, 17, 1102-1106.

[4] Sarkar, R.; Vasos, P. R.; Bodenhausen, G. *J. Am. Chem. Soc.* **2007**, 129, 328-334.

[5] Pileio, G.; Levitt, M. H. *J. Magn. Reson.* **2008**, 191, 148-155.

[6] Pileio, G.; Levitt, M. H. *J. Magn. Reson.* **2007**, 187, 141-145.

[7] Grant, A. K.; Vinogradov, E. *J. Magn. Reson.*, **2008**, 193, 177–190.

[8] Haeberlen, U. 'High resolution NMR in solids – selective averaging', *Adv. Magn. Reson.*, Supplement 1, New York Academic Press, **1976**, p. 153.

[9] Mehring, M. 'Principles of high resolution NMR in solids' second edition; Springer-Verlag, **1983**.

[10] Ahuja, P.; Sarkar, R.; Vasos P. R.*J. Chem. Phys.*, **2007**, 127, 134112.

[11] M. Karplus,*J. Am. Chem. Soc.*, **1963**, 85, 2873.

[12] A. DeMarco, M. Llinás, K. Wüthrich,*Biopolymers*, **1978**, 17, 617-636.

[13] Al-Karaghouli, A. R.; Koetzle, T. F. *Acta Cryst.*, **1975**, B31, 2461–2465.

[14] Wolfram Research, Inc.; *Mathematica* Version 7.0, Champaign IL, (2008).

[15] M. H. Levitt; "mPackages: a set of *Mathematica* routines for various 3D objects, Euler angles and frame transformations, Wigner matrices and Clebsch-Gordon coefficients, spin operators and superoperators, and symmetry-based pulse sequence analyses", Version 5.09, available online.

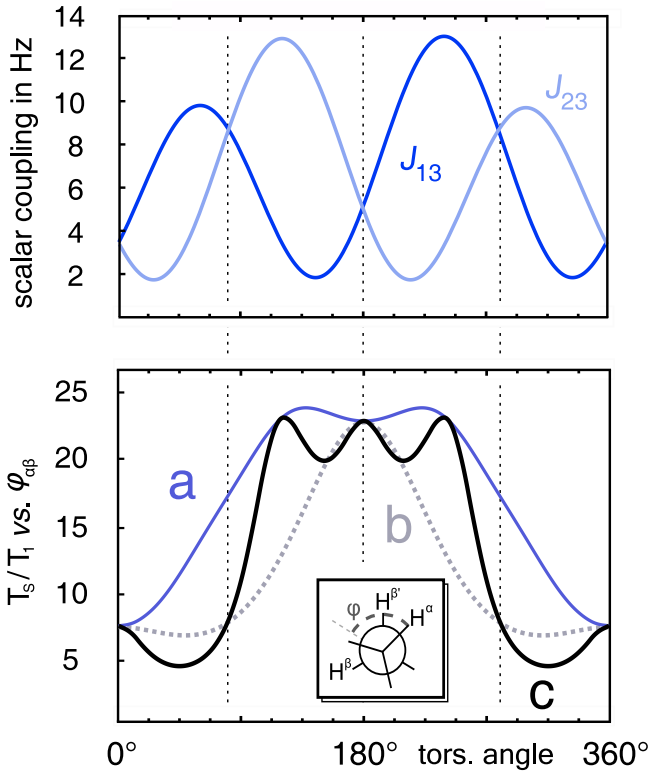

Figure 3: Liouvillian eigenvalues corresponding to the longest-lived *singlet* population operator $N[|S_0^{12}\rangle\langle S_0^{12}| - \frac{1}{3}(|T_{-1}^{12}\rangle\langle T_{-1}^{12}| + |T_0^{12}\rangle\langle T_0^{12}| + |T_{+1}^{12}\rangle\langle T_{+1}^{12}|)]$ are displayed as a function of the d_1-Phe three-spin geometry for several models of the relaxation: In the lower figure, curve (a) shows the Liouvillian eigenvalue analysis including all pair DD couplings, but no scalar coupling between the protons. Here the eigenvector is in general a linear combination of singlet states from all three proton pairings; (b) then includes the scalar coupling between nuclei 1 and 2, $J_{\beta\beta'} = -14.5$ Hz, typical of the experimental value, and this curve is identical to the result obtained using the first-order perturbation formulas. The effect of this J coupling is to localize the long-lived population on the CH_2 singlet; in (c), influences of the scalar coupling to the H^α spin are incorporated, where the torsional-angle dependence takes Wüthrich's parameterization for the ${}^\beta CH_2{}^\alpha CH$ spin systems of an amino acid within a random-coil peptide chain (*viz.* $J_{\alpha\beta} = 9.4\cos^2(\varphi + 60°) - 1.6\cos(\varphi + 60°) + 1.8$: [11, 12]). Note between approximately $\varphi = [-90°, 90°]$ the singlet relaxation rate actually becomes *slower* than of the previous model. The intersections between curves (b) and (c) match with the points where $J_{\alpha\beta} - J_{\alpha\beta'} = 0$, as discussed by Pileio *et al.* [6].